THE JOURNAL OF BIOLOGICAL CHEMISTRY VOL. 291, NO. 38, pp. 20113–20124, September 16, 2016

The Receptor Site and Mechanism of Action of Sodium Channel Blocker Insecticides*[S]

Received for publication, June 6, 2016, and in revised form, July 18, 2016 Published, JBC Papers in Press, August 3, 2016, DOI 10.1074/jbc.M116.742056

Yongqiang Zhang[‡§1], Yuzhe Du[§], Dingxin Jiang[§1,2], Caitlyn Behnke[§], Yoshiko Nomura[§], Boris S. Zhorov[¶‖3], and Ke Dong[§4]

From the [‡]College of Plant Protection, Southwest University, Chongqing 400716, China, the [§]Department of Entomology, Genetics and Neuroscience Programs, Michigan State University, East Lansing, Michigan 48824, the [¶]Department of Biochemistry and Biomedical Sciences, McMaster University, Hamilton, Ontario L8S 4K1, Canada, and the [‖]Sechenov Institute of Evolutionary Physiology and Biochemistry, Russian Academy of Sciences, St. Petersburg 194223, Russia

Sodium channels are excellent targets of both natural and synthetic insecticides with high insect selectivity. Indoxacarb, its active metabolite DCJW, and metaflumizone (MFZ) belong to a relatively new class of sodium channel blocker insecticides (SCBIs) with a mode of action distinct from all other sodium channel-targeting insecticides, including pyrethroids. Electroneutral SCBIs preferably bind to and trap sodium channels in the inactivated state, a mechanism similar to that of cationic local anesthetics. Previous studies identified several SCBI-sensing residues that face the inner pore of sodium channels. However, the receptor site of SCBIs, their atomic mechanisms, and the cause of selective toxicity of MFZ remain elusive. Here, we have built a homology model of the open-state cockroach sodium channel BgNa$_v$1-1a. Our computations predicted that SCBIs bind in the inner pore, interact with a sodium ion at the focus of P1 helices, and extend their aromatic moiety into the III/IV domain interface (fenestration). Using model-driven mutagenesis and electrophysiology, we identified five new SCBI-sensing residues, including insect-specific residues. Our study proposes the first three-dimensional models of channel-bound SCBIs, sheds light on the molecular basis of MFZ selective toxicity, and suggests that a sodium ion located in the inner pore contributes to the receptor site for electroneutral SCBIs.

Voltage-gated sodium channels are transmembrane proteins whose activation triggers fast inflow of sodium ions into the cell, causing the rising phase of the action potential. Eukaryotic voltage-gated sodium channels comprise the pore domain and four voltage-sensing domains within a single polypeptide chain of four homologous repeats. Each repeat includes six transmembrane helical segments (S1–S6) connected by extra- and intracellular loops. A voltage-sensing domain contains helices S1–S4. The pore domain is formed by quartets of the outer helices (S5s), the pore-lining inner helices (S6s), and extracellular membrane re-entering P-loops, which are contributed by the four repeats. The voltage-sensing domains are connected to the pore domain by linker helices S4-S5 (L45). Upon membrane depolarization, the positively charged helices (S4s) move outward, inducing opening of the activation gate, which is formed by cytoplasmic parts of the S6s. The selectivity filter is composed of Asp, Glu, Lys, and Ala residues from the ascending parts of the four P-loops and divides the ion-conducting pathway into the following two parts: the outer pore, which is exposed to the extracellular space, and the inner pore, which in the open channel is exposed to the cytoplasm.

Sodium channels are excellent targets of both natural and synthetic insecticides. Several classes of sodium channel-targeting insecticides are highly insecticidal, but less toxic to mammals and are widely used for controlling arthropod pests and human disease vectors (1). Pyrethroids are a large class of synthetic compounds structurally derived from pyrethrins and are broadly used for control of mites, ticks, and other insect pests. The sodium channel blocker insecticides (SCBIs),[5] indoxacarb and metaflumizone (MFZ) (Fig. 1), are among the relatively new classes of insecticides with favorable selectivity (1–3). The selective toxicity of indoxacarb is due to insect-specific metabolism that decarboxylates indoxacarb to produce a more toxic derivative, DCJW (3). However, the mechanism of selective toxicity of MFZ is still unknown.

The major problem for the effective use of insecticides is the development of insecticide resistance. Intensive use of pyrethroids over the last decades has led to selection of numerous mutations in sodium channels in various arthropod populations, which confer resistance to pyrethroids (4). Identification of these sodium channel mutations has facilitated the development of molecular markers for early detection of pyrethroid resistance in various populations around the world (5). Furthermore, these mutations help define the receptor sites for pyrethroids on sodium channels and reveal the molecular mechanisms of the differential sensitivities of insect and mammalian sodium channels to pyrethroids (6).

* This work was supported in part by National Institutes of Health Grant GM057440 from NIGMS (K. D. and B. S. Z.) and Natural Sciences and Engineering Research Council of Canada Grant RGPIN-2014-04894 (to B. S. Z.). The authors declare that they have no conflicts of interest with the contents of this article. The content is solely the responsibility of the authors and does not necessarily represent the official views of the National Institutes of Health.

[S] This article contains supplemental Figs. S1–S4.

[1] Supported by the China Scholar Council.

[2] Present address: Key Laboratory of Natural Pesticide and Chemical Biology, Ministry of Education, Laboratory of Insect Toxicology, South China Agricultural University, Guangzhou, China.

[3] To whom correspondence may be addressed. Tel.: 905-525-9140 (Ext. 22049); Fax: 905-522-9033; E-mail: zhorov@mcmaster.ca.

[4] To whom correspondence may be addressed. Tel.: 517-432-2034; Fax: 517-353-4354; E-mail: dongk@msu.edu.

[5] The abbreviations used are: SCBI, sodium channel blocker insecticide; LA, local anesthetic; MC, Monte Carlo; MCM, Monte Carlo energy minimization; MFZ, metaflumizone.

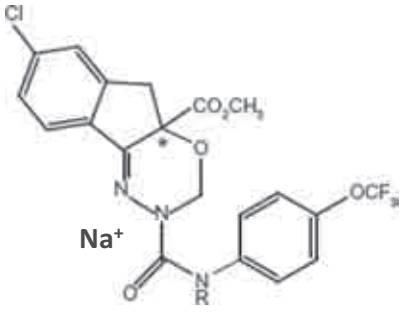

R=H, DCJW
$R=CO_2CH_3$, Indoxacarb

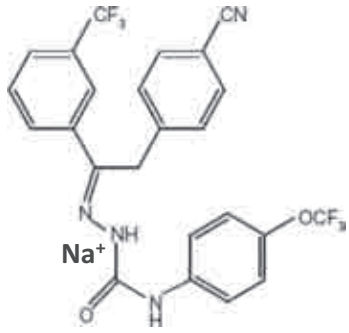

Metaflumizone (MFZ)

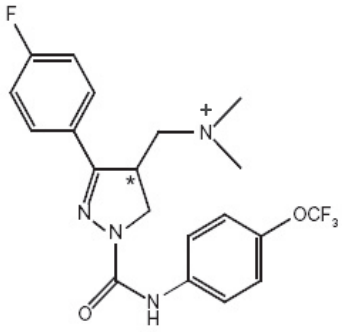

Compound D

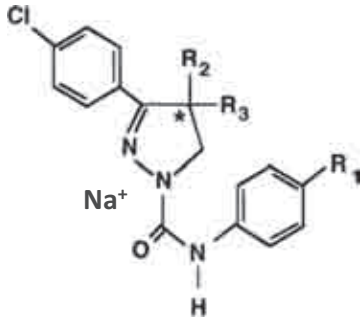

Compound	R_1	R_2	R_3
RH 4841	Cl	phenyl	H
RH 5654	Cl	phenyl	butyl
RH 7842	Cl	CO_2CH_3	CH_3
RH 3421	CF_3	CO_2CH_3	CH_3
RH 5529	H	CO_2CH_3	CH_3
RH 2643	CF_3	CO_2H	CH_3

FIGURE 1. **Structural formulae of SCBIs.** A sodium ion is placed at the possible position in the 5-membered chelating ring. In a low-potent compound D, the ammonium group is attracted to the imino nitrogen, making unlikely chelation of a sodium ion. The different positions of the ammonium nitrogen *versus* that of a chelated sodium in other compounds may explain the low potency of compound D. Structural formulae of compounds D and RH are taken from Refs. 2, 36.

Resistance to SCBIs recently emerged in populations of various agricultural pests. Two mutations, F1845Y and V1848I, in the sodium channel of the diamondback moth, *Plutella xylostella* (7), have been confirmed to reduce the SCBI sensitivity of cockroach sodium channels expressed in *Xenopus* oocytes (8). Therefore, the two mutations could be used as molecular markers for resistance monitoring in-field populations of the diamondback moth and possibly other pest species. Identification of more residues that are critical for the binding and action of SCBIs would provide further molecular markers for more accurate and earlier detection of resistance genotypes and might delay the development of resistance in natural populations.

SCBIs are believed to bind to and trap sodium channels in non-conducting slow inactivated states (9), the mechanism similar to that proposed for local anesthetics (LAs) (1, 10). Molecular interactions of LAs with mammalian sodium channels have been intensively studied (11, 12). Furthermore, structural models of the $Na_v1.4$ channel are elaborated in which several pore-facing residues in the inner helix IVS6 contribute to the binding site of LAs (13, 14). In particular, two LA-sensing residues in IVS6, *i.e.* Phe-1764 and Tyr-1771 in rat $Na_v1.2$ and Phe-1579 and Tyr-1586 in $Na_v1.4$, are consistently critical for the binding and action of a wide range of LAs and related drugs on mammalian sodium channels. To facilitate recognition of ligand-sensing residues among different sodium channels, here we labeled these two LA-sensing residues in IVS6 as F^{4i15} and Y^{4i22} using a nomenclature universal for P-loop ion channels (6, 15). Similar to the effect on the action of LAs, alanine substitution, $F^{4i15}A$, resulted in a significant reduction in the ability of DCJW and an experimental SCBI, RH3421, to inhibit $Na_v1.4$ sodium channels expressed in *Xenopus* oocytes (16). However, the same substitution $F^{4i15}A$ in a cockroach sodium channel, $BgNa_v1\text{-}1a$, did not reduce the potency of both DCJW and metaflumizone (17). Remarkably, one of the two mutations from the indoxacarb-resistant diamondback moth populations was a tyrosine substitution of F^{4i15}, which reduced the action of

both DCJW and metaflumizone on $BgNa_v1$-1a channels expressed in *Xenopus* oocytes (7, 8). Furthermore, mutation of the tyrosine residue, Y^{4i22}, to alanine in $Na_v1.4$ channels resulted in a significant increase in the potency of indoxacarb, DCJW, and RH3421 (16), and the same substitution, $Y^{4i22}A$, also enhanced the action of metaflumizone on $BgNa_v1$-1a channels (17). These data strongly support the notion that SCBI receptors are located, at least partially, in the inner pore and may overlap with the LA receptors (2). However, specific atomic details of interactions between SCBIs with sodium channels are still unclear.

In this study, we generated an open-state model of the cockroach sodium channel, $BgNa_v1$-1a. The model has the wide open activation gate like in the x-ray structure of the open potassium channel $K_v1.2$ (18) and wide inter-repeat fenestrations like in the x-ray structure of the closed sodium channel Na_vAb (19). SCBIs are bigger and have more electronegative atoms than LAs like lidocaine. At physiological pH, LAs are protonated to bear a positive charge that enables the channel block by electrostatic mechanism (13, 14). In contrast, SCBIs are electrically neutral non-ionizable compounds (Fig. 1). Driven by the hypothesis that certain electroneutral compounds and permeant ions may form cationic blocking particles (20), we docked sodium-bound DCJW and MFZ into the channel. We arrived at a model in which the bulky part of SCBIs binds in the inner pore, a halogenated aromatic moiety protrudes in the III/IV fenestration, and the ligand-bound sodium ion occurs in the cation-attractive region of the inner pore, at the focus of P1 helices. Model-driven mutational and electrophysiological analyses revealed five new SCBI-sensing residues. These include insect-specific residues in the III/IV repeat interface and at the turn of repeat IV P-loop. We also revealed residues that interact with either MFZ or DCJW. Our study provides atomic details of the MFZ and DCJW receptors and supports the hypothesis on direct interactions of permeant cations with electroneutral ligands of ion channels (20). These results contribute to better understanding of mechanisms of sodium channel modulation by various ligands and will assist in monitoring emerging SCBI resistance of pests and rational design of new SCBIs.

Results

Open-state Model of $BgNa_v1$-1a—Previously identified SCBI-sensing residues F^{4i15}, V^{4i18}, and Y^{4i22} (Fig. 2) face the inner pore (8), and F^{4i15} may also face the III/IV fenestration (21). None of the currently available high resolution structures of P-loop channels can be directly used to build a homology model of the open sodium channel, which would be suitable for the computational search for binding sites of large SCBI molecules. Indeed, the x-ray structures of the closed sodium channels (19, 22, 23) have wide fenestrations between two S6 and P1-helix, but their narrow S6 bundle is a poor template to model the cytoplasmic half of the open inner pore. The x-ray structures of open potassium channels, *e.g.* $K_v1.2$ (18) have the wide inner pore, but their narrow inter-subunit interfaces are poor templates to model the wide fenestrations. The open-state structure of a prokaryotic sodium channel, Na_vMs (24), lacks the linker-helices S4-S5, which contribute to the binding sites of pyrethroids and 1,1,1-trichloro-2,2-bis(*p*-chlorophenyl)ethane and, *a priori*, could also participate in the binding of SCBIs. Moreover, the cytoplasmic half of the inner pore in Na_vMs is narrower than that in $K_v1.2$ (the distance between diagonally opposed atoms C^{β}_i19 in Na_vMs and $K_v1.2$ are 12.9 and 14.0 Å, respectively).

To resolve the problem, we *in silico* opened a Na_vAb-based model of the closed mosquito sodium channel $AaNa_v1$-1a (6), see under "Materials and Methods" and supplemental Fig. S1. Residues of the $AaNa_v1$-1a and $BgNa_v1$-1a channels within the inner pore and repeat interfaces are practically identical. Therefore, we call the obtained model the $Na_vAb/K_v1.2$-based model of the open $BgNa_v1$-1a channel. This model has a wide III/IV fenestration and a wide open activation gate (supplemental Fig. S2, *A* and *B*). The known SCBI-sensing residues F^{4i15}, V^{4i18}, and Y^{4i22} face the inner pore (supplemental Fig. S2, *C* and *D*).

Docking DCJW into the Open $BgNa_v1$-1a Channel—We first docked DCJW in the sodium ion-free channel as described under "Materials and Methods." In the apparent global minimum and several local minima, the heterocyclic core of DCJW bound against the IVS6 inner helix forming close contacts with F^{4i15}, V^{4i18}, and Y^{4i22}, whereas aromatic moieties at the opposed termini of the ligand approached the III/IV and I/IV fenestrations (supplemental Fig. S3). The model is consistent with the results from mutational analysis of the action of DCJW on $rNa_v1.4$ and $BgNa_v1$-1a channels (Table 1). However, it highlights three issues. First, there is a large imbalance between the number of polar atoms in DCJW and in the side chains of pore-facing residues. Indeed, the central part of DCJW contains seven closely spaced oxygen and nitrogen atoms (Fig. 1), but their binding partners in the channel are unknown. In the model, only tyrosine Y^{4i22} approached DCJW but did not H-bond to it. Other polar residues, which face the inner pore (S^{1i15}, N^{2i15}, S^{3i15}, and Q^{1p49}), were too far from the DCJW heterocyclic core. Thus, the model does not explain the role of the N–N–C=O fragment, which is the "fingerprint" of SCBIs (Fig. 1). Second, both LAs and DCJW are believed to bind preferably to slow-inactivated channels (10, 16, 25). In the case of LAs, the preference is likely due to the lack of electrostatic repulsion between the ligand charged group and the cation-deficient outer pore (13). In the case of electroneutral DCJW, the cause of the preference is unclear. Third, the model does not suggest an atomic mechanism for the Na^+ current block by the ligand. DCJW, which binds tightly to the pore-lining helix IVS6, does not occlude the inner pore, leaving space for permeant ions to pass between the ligand and polar residues S^{1i15}, N^{2i15}, and S^{3i15} (supplemental Fig. S3). Such a binding mode is proposed for sodium channel agonists like batrachotoxin (26, 27), but cationic antagonists such as LAs block the permeation by the electrostatic mechanism (13, 14). The fact that cationic LAs and electroneutral DCJW have common pore-facing ligand-sensing residues F^{4i15}, V^{4i18}, and Y^{4i22} and that these ligands apparently target the same region in the inner pore is a paradox.

A possible solution to these three issues could be based on the hypothesis that electroneutral ligands block the cation-attractive pore of ion channels not *per se* but in complexes with permeant ions (20). We first explored whether DCJW can inter-

A

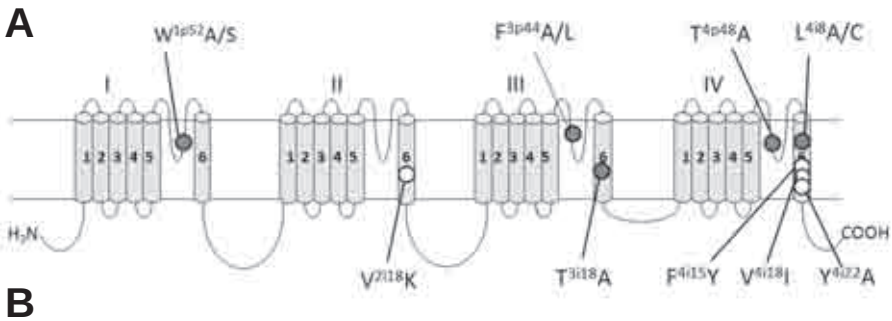

B

Channel	Segment	o1 | o11 | o21
K_v1.2	S5	ASMRELGLLI FFLFIGVILF SSAVYFAEA
NavAb	S5	SVIPGMLSVI ALMTLFFYIF AIMATQLFG
BgNa$_v$1-1	I S5	ESVKNLRDVI ILTMFSLSVF ALMGLQIYM
	II S5	RTVGALGNLT FVLCIIIFIF AVMGMQLFG
	III S5	QAIPSIFNVL LVCLIFWLIF AIMGVQLFA
	IV S5	MSLPALFNIC LLLFLVMFIF AIFGMSFFM
hNav1.4	I S5	QSVKKLSDVM ILTVFCLSVF ALVGLQLFM
	II S5	NSVGALGNLT LVLAIIVFIF AVVGMQLFG
	III S5	GAIPSIMNVL LVCLIFWLIF SIMGVNLFA
	IV S5	MSLPALFNIG LLLFLVMFIY SIFGMSNFA

		p33 | p41 | p51
K_v1.2	P	FPSIPDAF WWAVVSMTTV GYGDMVPT
NavAb	P	FGTLGESF YTLFQVMTLE SWSMGIVR
BgNa$_v$1-1	IP	CIKNFWAF LSAFRLMTQD YW.ENLYQ
	IIP	VERFPHSF MIVFRVLCGE .WIESMWD
	IIIP	STTLSKAY LCL**F**QVATFK GW.IQIMN
	IVP	GLDDVQSM ILLFQM**S**TSA GW.DGVLD
hNav1.4	IP	YDTFSWAF LALFRLMTQD YW.ENLFQ
	IIP	MHDFFHSF LIVFRILCGE .WIETMWD
	IIIP	YDNVGLGY LSL**L**QVATFK GW.MDIMY
	IVP	FETFGNSI ICLFEI**T**TSA GW.DGLLN

		i1 | i11 | i21
K_v1.2	S6	IGGKIVGSLC AIAGVLTIAL PVPVIVSNFN
NavAb	S6	PYAWVFFIPF IFVVTFVMIN LVVAICVDAM
BgNa$_v$1-1	IS6	PWHMLFFIVI IFLGSFYLVN LILAIVAMSY
	IIS6	WSCIPFFLAT VVIGNLVVLN LFLALLLSNF
	IIIS6	IYMYLYFVFF IIFGSFFTLN LFIGVIIDNF
	IVS6	TVGLAFL**L**SY **LV**ISFLIV**I**N MYIAVILENY
hNav1.4	IS6	KTYMIFFVVI IFLGSFYLIN LILAVVAMAY
	IIS6	AMCLTVFLMV MVIGNLVVLN LFLALLLSSF
	IIIS6	LYMYLYFVIF IIFGSFFTLN LFIGVIIDNF
	IVS6	SIGICFF**C**SY **II**ISFLIV**V**N MYIAIILENF

FIGURE 2. *A*, transmembrane topology of the BgNa$_v$1.1 channel. *Open circles* indicate SCBI-sensing residues that were identified in earlier studies. *Filled circles* indicate SCBI-sensing residues, which are identified in this study. *B*, sequence alignment of K_v1.2 and sodium channels. Positions of residues according to the universal labeling scheme of P-loop are indicated above aligned sequences of individual segments. Residues, which face the inner pore or III/IV fenestration and which are different between the insect and mammalian channels, are *underlined*. Insertion/deletions in the P-loops are shown according to the sequence alignment proposed in Ref. 50.

act with a sodium ion located at position Na_{III}, between the backbone carbonyls of residues p48 as seen in the Na$_v$Ms x-ray structure (24). We fixed a sodium ion in this position and submitted several MCM trajectories with various electronegative atoms of DCJW constrained to the sodium ion. These calculations did not yield a low energy complex with DCJW approaching the experimentally known DCJW-sensing residues F^{4i15} and V^{4i18}.

We then explored whether DCJW can interact with a sodium ion in the inner pore. In the x-ray structures of the open and closed potassium channels, a potassium ion is seen in the inner pore, at the focus of P-helices (18, 28). Because the exact position of a sodium ion in the inner pore is unknown, we considered many various possibilities as described below.

Docking Library of Sodium-bound DCJW Conformers—We generated a library of 110 sodium-bound DCJW conformers (supplemental Fig. S4). In most of the structures, the imino nitrogen and carbonyl oxygen chelated the sodium ion forming an energetically favorable five-membered chelating ring (29). In addition, many structures were found with the sodium ion che-

TABLE 1
Effects of mutations on the blockers' potency
The following symbols are used: ↑, more potent; ↓, less potent; and ≈, same.

Mutant	Channel	Ligand			Ref.
		DCJW	MFZ	LAs	
$W^{1p52}A$	$BgNa_v1$-1a	↓	↓		This study
$W^{1p52}S$	$BgNa_v1$-1a	↓	≈		This study
$V^{2i18}K$	rNav1.4	≈	↓		51
$F^{3p44}L$	$BgNa_v1$-1a	↓	≈		This study
$F^{3p44}A$	$BgNa_v1$-1a	↓	↓		This study
$T^{3i18}A$	$BgNa_v1$-1a	≈	↓		This study
$T^{4p48}A$	$BgNa_v1$-1a	↓	≈		This study
$L^{4i8}A$	$BgNa_v1$-1a	↓	↓		This study
$L^{4i8}C$	$BgNa_v1$-1a	≈	≈		This study
$F^{4i15}A$	$Na_v1.4$	↓	↓	↓	52, 53
$F^{4i15}A$	$BgNa_v1$-1a	≈	↑		17
$F^{4i15}Y$	$BgNa_v1$-1a	↓	↓	↓	8
$V^{4i18}I$	$BgNa_v1$-1a	↓	↓	↓	8
$V^{4i18}A$	$BgNa_v1$-1a	≈	↑	↑	8
$Y^{4i22}A$	$rNa_v1.4$	↑	↑	↓	52, 53
$Y^{4i22}A$	$BgNa_v1$-1a	↑	↑		17

lated between an aromatic ring and a carbonyl oxygen. For each sodium-bound DCJW conformer, 256 random starting positions/orientations in the inner pore were generated, and the starting points were MC-minimized. The *in silico* opened homology model of the pseudo-heteromeric eukaryotic channel is not expected to be precise enough to use energetics as the only criterion to select the specific binding mode. Therefore, we imposed distance constraints between DCJW and DCJW-sensing residues F^{4i15} and V^{4i18} to bias the docking and find a compromise between the computed energetics and the experimental data.

In the lowest energy complex (Fig. 3), the sodium ion was bound to two nitrogen and two oxygen atoms of DCJW. The ion occurred in the central cavity, at the level of the pore-facing residues S^{1i15}, N^{2i15}, S^{3i15}, and F^{4i15}. These residues are highly conserved in eukaryotic sodium channels and likely contribute to intermediate binding site(s) for hydrated permeant ions. The DCJW-distant hemisphere of the sodium ion faced N^{2i15} and S^{3i15} and would attract water molecules wetting these residues. The summed electronegative potentials from the C-ends of P1-helices would further stabilize the DCJW-bound sodium ion and thus the entire channel-blocking cationic particle. The dihydroindene moiety formed a stacking contact with F^{4i15} and closely approached V^{4i18}. Tyrosine Y^{4i15} directed toward the carbonyl oxygen in the bridge between two cyclic moieties but was too far to donate an H-bond to DCJW. The chlorine atom extended into the III/IV interface and interacted with F^{3p44} and L^{4i8}, which are insect-specific residues (Fig. 2). The phenyl trifluoromethyl group at the other end of DCJW approached T^{4p48}. The latter forms an interdomain H-bond with W^{1p52} (19) that contributes to the stability of the P-loop domain.

Docking Library of Sodium-bound MFZ—MFZ and DCJW have common ligand-sensing residues F^{4i15} and V^{4i18} (8) and a common fragment C=N–NH–C=O that may chelate a sodium ion. We generated a library of 140 sodium-bound MFZ conformers that contained highly divergent structures (supplemental Fig. S4, *E* and *F*). In the lowest energy complex the ion was chelated by the carbonyl oxygen and the imino nitrogen with the involvement of π-electrons from an aromatic ring (supplemental Fig. S4*F*). For each sodium-bound MFZ conformer, 256 random starting positions/orientations in the inner pore were generated, and the starting points were MC-minimized with distance constraints between the ligand and known MFZ-sensing residues V^{2i18}, F^{4i15}, V^{4i18}, and Y^{4i22}.

The lowest energy ternary complex MFZ/Na^+/$BgNa_v1$-1a is shown in Fig. 4. The imino nitrogen and the carbonyl oxygen chelated a sodium ion in the central cavity, at the focus of P1-helices. As in the case of DCJW, the MFZ-distant sodium ion hemisphere faced N^{2i15} and S^{3i15} and would interact with water molecules wetting these residues. The trifluoromethoxy-phenyl moiety stacked with F^{4i15} and extended into the III/IV interface to reach the insect-specific F^{3p44} and I^{4i8}, and this moiety also approached T^{3i18}. The trifluoromethyl-phenyl moiety extended toward IIS6 to reach the MFZ-sensing V^{2i18}. The 4-cyanophenyl group extended toward the I/II interface. Thus, our calculations predicted new SCBIs sensing residues that are common for MFZ and DCJW (F^{3p44} and I^{4i8}), a DCJW-specific T^{4p48}, and an MFZ-specific residue T^{3i18}.

Na_vMs-based Model of $BgNa_v1$-1a with SCBIs—Our computations did not reveal SCBI-binding residues in the S4-S5 linkers or at the S5 and S6 sides that face the linkers. Therefore, the Na_vMs x-ray structure, which lacks the S4-S5 linkers, appears suitable for computational docking of SCBIs. We used MCM to move C^α atoms of $Na_vAb/K_v1.2$-based model to positions of respective atoms in the Na_vMs x-ray structure as described elsewhere (30). In the obtained model, positions of the S4-S5 helices are similar to those in the $Na_vAb/K_v1.2$-based model. DCJW fits snugly in the Na_vMs-based model and forms contacts with the same residues as in the $Na_vAb/K_v1.2$-based model (Fig. 5). We used the same approach to obtain Na_vMs-based model of $BgNa_v1$-1a with MFZ and also found that MFZ forms contacts with the same residues as in the $Na_vAb/K_v1.2$-based model (data not shown).

Mutational Studies Are Consistent with the Predicted Binding Sites of DCJW and MFZ—We used an SCBI-sensitive cockroach sodium channel, $BgNa_v1$-1a (17), to generate six mutants of the four predicted SCBI-sensing residues that directly interact with SCBI in our models. We also generated two mutants of W^{1p52}, which did not interact with SCBIs in our models but forms interdomain H-bonds with the predicted DCJW-sensing residue T^{4p48}. We expressed the eight mutants individually in oocytes and examined the effect of the mutations on the action of SCBIs. Most of the mutations did not alter the voltage dependence of activation, fast inactivation, or slow inactivation (Table 2). As shown previously (8, 17), DCJW and metaflumizone cause state-dependent inhibition of $BgNa_v1$-1a channels at depolarized holding potentials during 30 min of insecticide exposure (Fig. 6). The inhibition of sodium currents by DCJW at the end of 30 min of the insecticide exposure was significantly reduced by mutations $F^{3p44}A$, $F^{3p44}L$, $L^{4i18}A$, $W^{1p52}A$, $W^{1p52}S$, and $T^{4p48}A$ but not by $L^{4i18}C$ or $T^{3i18}A$ (Figs. 6 and 7 and Table 3). We then examined the action of MFZ on the same mutants. Mutations of four residues ($F^{3p44}A$, $L^{4i18}A$, $W^{1p52}A$, and $T^{3i18}A$) did decrease the potency of MFZ. Mutation $T^{4p48}A$ had no effect on the MFZ action.

Discussion

DCJW and MFZ-binding Sites—In this study we have built open-state models of the $BgNa_v1$-1a channel, docked DCJW

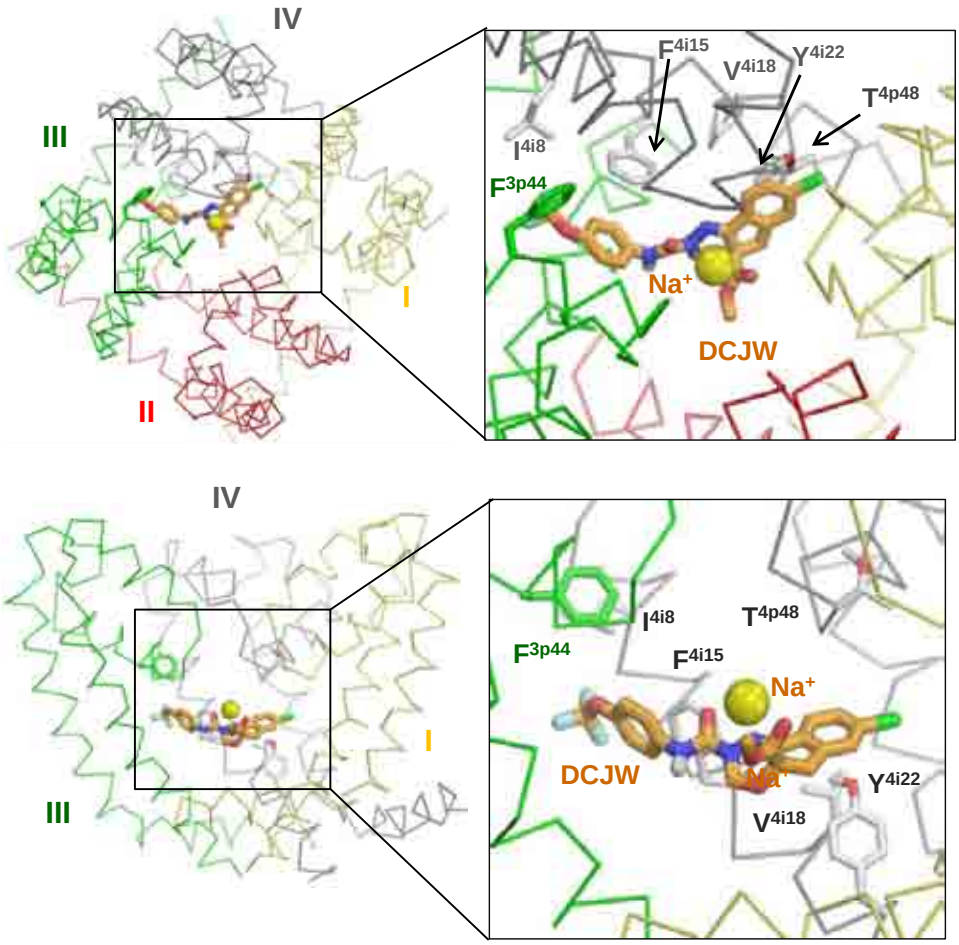

FIGURE 3. **Sodium-bound DCJW in the Na_vAb/K_v1. 2-based model of $BgNa_v1$-1a.** *Top,* extracellular view and its enlargement. *Bottom,* side view and its enlargement with domain II removed for clarity. Backbones in repeat domains I, II, III, and IV are shown by C^{α} tracings colored *yellow, red, green,* and *gray*, respectively. The side chains of DCJW-sensing residues are shown by *sticks*, which are colored as respective backbones. See "Results" for further details.

and MFZ, and used model-driven mutagenesis and electrophysiology to map binding sites for these SCBIs. A channel mutation may affect ligand action directly, by changing the ligand-channel contacts or indirectly by changing the channel conformation and thus the state-dependent binding-site geometry. For example, tryptophans in positions p52 are exceptionally conserved in sodium and calcium channels. They form intersubunit H-bonds with threonines p48 (19) and are involved in other intersegment contacts that stabilize folding of the P-loop domain (31). Despite that W^{1p52} does not form direct contacts with SCBIs in our models (Fig. 5), mutation $W^{1p52}A$ decreased the potency of DCJW and MFZ (Figs. 6 and 7) likely due to destabilizing folding of the P-loop domain that contributes to the SCBI-binding sites. However, it is unlikely that mutations of residues, which form direct contacts with SCBIs in our models, indirectly affected action of the ligands.

Although the current reduction by the mutants is rather small (Fig. 7), it should be noted that the effects are comparable with those of naturally occurring kdr mutations $F^{4i15}Y$ and $I^{4i18}I$ that are found in diamondback moth (*P. xylostella*) in China (7) and demonstrated to reduce action of SCBIs in $BgNa_v1$-1a (8).

Previous studies revealed four SCBI-sensing residues in the $BgNa_v1$-1a and $Na_v1.4$ channels (Table 1). These experimental data along with the hypothesis on direct interaction of electroneutral blockers of ion channels with the permeant ions (20) were used to focus our search for the SCBI-binding sites. We arrived to the models where sodium-bound ligands bind tightly against IVS6, approach the P-loops in repeats I and III, and extend a hydrophobic group into the III/IV interface. Our model-driven mutagenesis unveiled five previously unknown DCJW and MFZ-sensing residues, including the insect-specific residues F^{3p44} and L^{4i8}, as well as residues that individually contribute to the receptors of DCJW (T^{4p48}) and MFZ (T^{3i18}). The fact that mutations of the insect-specific residues F^{3p44} and $L^{4i8}A$ (Fig. 7*B*) affect the MFZ action may explain the selective toxicity of MFZ. The previous finding that the $V^{2i18}K$ mutation in $rNa_v1.4$ significantly reduces the action of MFZ, but has no effect on the action of DCJW (Table 1), is consistent with our models where tri-polar MFZ, but not dipolar DCJW, reached IIS6.

Unlike other SCBIs, MFZ can bind to the resting sodium channels (2). The long predicted hydrophobic access pathway for LAs in the closed sodium channels (25) was first visualized in homology models of sodium channels where LAs are proposed to reach the closed sodium channels through the "sidewalk" in the III/IV repeat interface (21, 32). The x-ray crystallography demonstrated a wide inter-subunit fenestration in a prokaryotic sodium channel Na_vAb (19) in the same location as

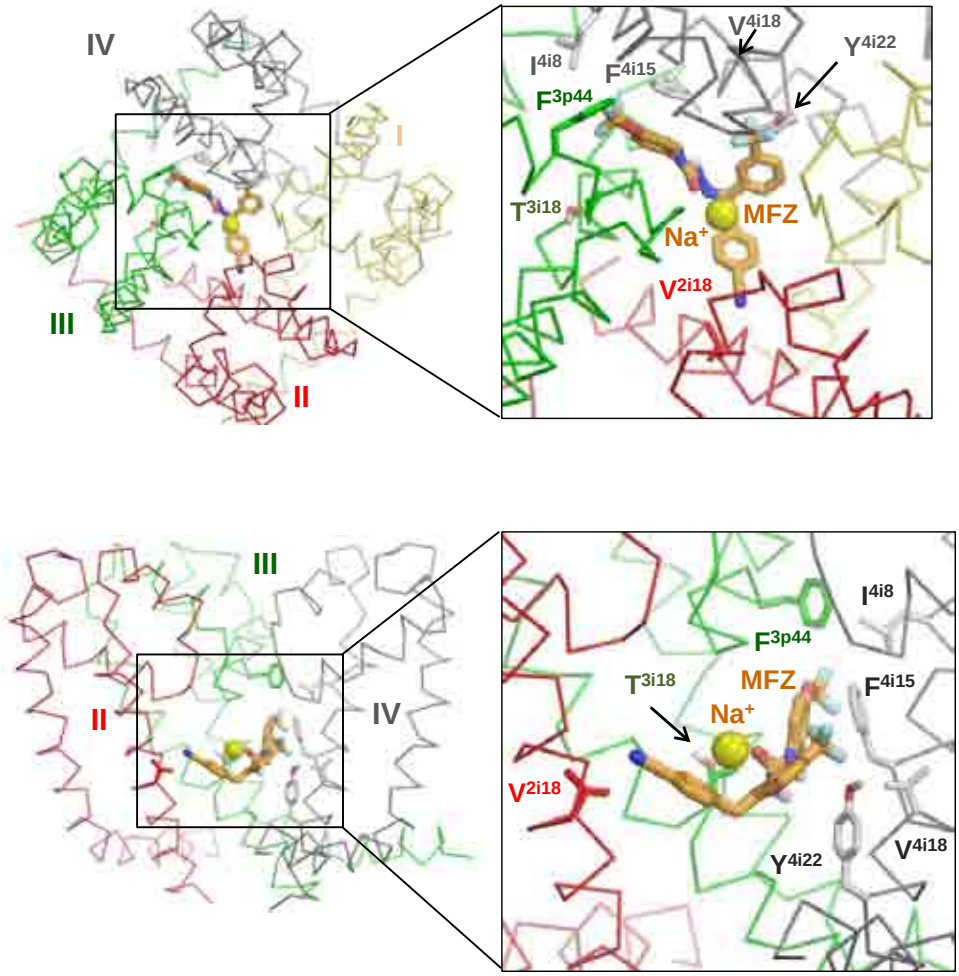

FIGURE 4. **Sodium-bound MFZ in the Na_vAb/K_v1. 2-based model of $BgNa_v1$-1a.** *Top,* extracellular view and its enlargement. *Bottom,* side view and its enlargement with domain II removed for clarity. Backbones and side chains are colored as in Fig. 3. See "Results" for further details.

the predicted sidewalk in the eukaryotic channels. Here we revealed two MFZ-sensing residues, F^{3p44} and L^{4i8}, in the III/IV fenestration (Table 1). In view of these data, we suggest that a highly flexible MFZ molecule would pass through the III/IV fenestration in the resting (closed) channel and block it. DCJW has the bulky tricyclic core and is much more rigid than MFZ. In addition, DCJW has three more oxygen atoms than MFZ (Fig. 1). These two factors may explain why the hydrophobic access pathway involving the membrane and the III/IV fenestration is impassible for DCJW.

SCBI Action in Insect and Mammalian Channels—Mutation $F^{4i15}A$ significantly impairs the action of DCJW and MFZ in the $rNa_v1.4$ channel, but it does not affect the action of DCJW or enhance the action of MFZ in $BgNa_v1$-1a (Table 1). These facts indicate that SCBI receptors in the $Na_v1.4$ and $BgNa_v1$-1a channels are not identical (2). In our models, SCBIs would be attracted to big hydrophobic residues F^{3p44} and L^{4i8} in $BgNa_v1$-1a more strongly than to their smaller cognates L^{3p44} and C^{4i8} in $rNa_v1.4$ (Table 4). In two other fenestration-lining positions, *4i11* and *4i12*, the $Na_v1.4$ channel has isoleucines, whereas $BgNa_v1$-1a has smaller valines (Fig. 2 and Table 4). These facts suggest that the trifluoromethoxy-phenyl moiety of the flexible MFZ would penetrate more deeply into the III/IV fenestration of $BgNa_v1$-1a than into the cognate fenestration of $Na_v1.4$. The deeper MFZ penetration would be opposed by the pore-facing F^{4i15}. Mutation $F^{4i15}A$ would permit the flexible MFZ deeper into the III/IV fenestration (which is also lined by the MFZ-sensing T^{3i18}). In contrast, the more rigid DCJW would be unable to move more deeply into the III/IV fenestration, and the $F^{4i15}A$ mutation would not affect its action.

The fact that mutations $V^{4i18}I$ and $F^{4i15}Y$ decrease the potency of both MFZ and DCJW in the $BgNa_v1$-1a channel (Table 1) is consistent with our models that suggest tight binding of the ligands against IVS6. The bigger $V^{4i18}I$ would sterically repel the ligand, whereas the hydroxyl group in $F^{4i15}Y$ would repel the hydrophobic moieties of the ligand. Mutation $Y^{4i22}A$ potentiates DCJW and MFZ block in both $rNa_v1.4$ and $BgNa_v1$-1a (Table 1). In our models, the side chain of Y^{4i22} is oriented upward and its hydroxyl group approaches hydrophobic moieties of the ligands. This energetically unfavorable interaction would be relieved in the $Y^{4i22}A$ mutant.

The above rationale suggests that the binding modes of SCBIs in the $rNa_v1.4$ and $BgNa_v1$-1a channels are similar, whereas different effects of the $F^{4i15}A$ mutation are due to channel-specific residues in the III/IV fenestrations. However, our homology models are not precise enough to quantitatively evaluate the energetics of SCBI interactions in different channels and their mutants.

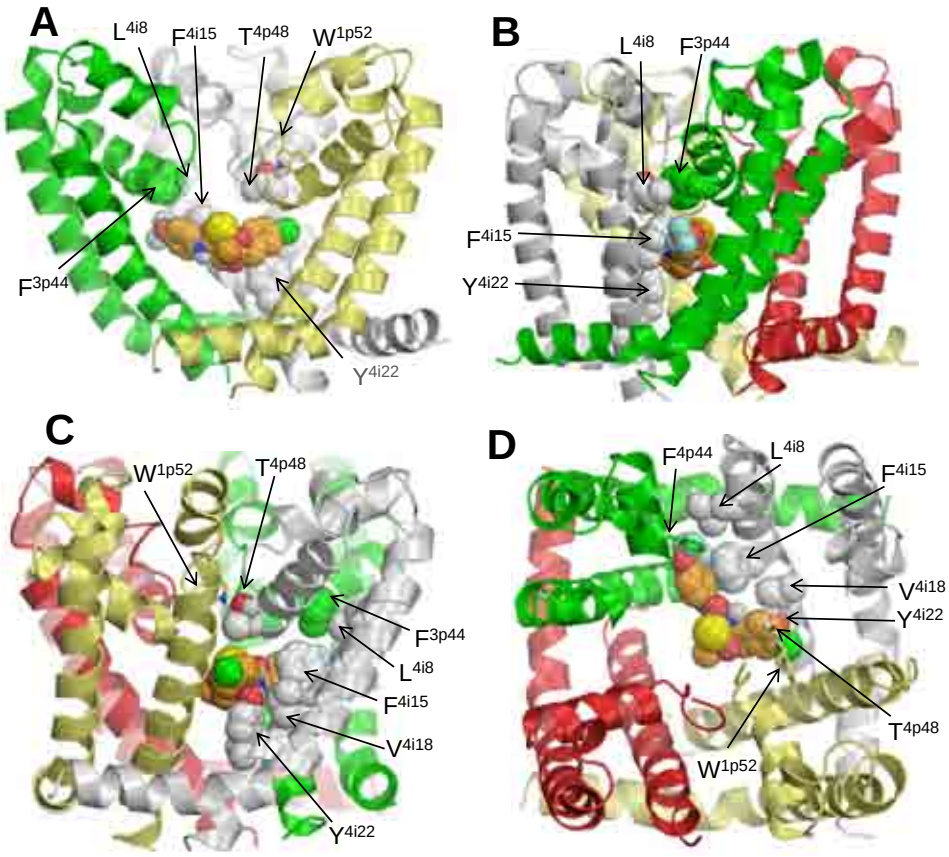

FIGURE 5. **Na_vMs-based model of the open $BgNa_v1$-1a channel with sodium-bound DCJW docked as in the $Na_vAb/K_v1.2$ based model.** The pore domain helices are shown as *ribbons*. DCJW and DCJW-sensing residues are shown as *spheres* with hydrogen atoms removed for clarity. *A*, side view with removed domain IV. *B*, view through the III/IV fenestration. Note that DCJW binds tightly against DCJW-sensing residues F^{4i15}, V^{4i18}, and Y^{4i22} and forms close contacts with insect-specific residues F^{3p44} and L^{4i8}. *C*, view through the IV/I fenestration. *D*, view from the extracellular side with parts of P-loops removed for clarity.

TABLE 2

Voltage dependence of activation, fast, and slow inactivation of $BgNa_v1$-1a and mutant channels at the holding potential of −120 mV

The voltage dependences of conductance and inactivation were fitted with a two-state Boltzmann equation to determine $V_{1/2}$, the voltage for half-maximal conductance or inactivation, and k, the slope factor for conductance or inactivation. The number of oocytes was 6–14, and values in the table represent the mean ± S.E. The asterisks indicate significant differences from the $BgNa_v1$-1a channel as determined by one-way analysis of variance ($p<0.05$) with Scheffe's post hoc analysis. Asterisks indicate that the specific residue lines the inner pore and/or specific fenestration.

	Activation		Fast inactivation		Slow inactivation	
Na^+ channel	$V_{1/2}$	k	$V_{1/2}$	k	$V_{1/2}$	k
	mV		*mV*		*mV*	
$BgNa_v1$-1a	−28.2 ± 0.3	5.1 ± 0.9	−49.0 ± 0.4	4.2 ± 0.1	−54.6 ± 0.9	4.2 ± 0.2
$F^{3p44}A$	−22.7 ± 1.5	5.4 ± 0.2	−51.4 ± 0.8	4.5 ± 0.2	−55.3 ± 2.1	9.8 ± 0.7
$F^{3p44}L$	−34.7 ± 1.3	2.6 ± 0.3	−51.4 ± 0.9	4.4 ± 0.1	−59.6 ± 2.7	5.9 ± 0.6
$L^{4i8}A$	−43.1 ± 1.7*	2.8 ± 0.3	−44.2 ± 0.6*	4.9 ± 0.3	−50.6 ± 0.4	5.4 ± 0.5
$L^{4i8}C$	−32.5 ± 1.4	4.1 ± 0.3	−43.2 ± 1.1*	3.9 ± 0.2	−57.2 ± 2.6	5.1 ± 0.8
$W^{1p52}A$	−29.8 ± 1.9	3.9 ± 0.4	−50.7 ± 0.7	4.3 ± 0.9	−66.3 ± 1.5*	6.2 ± 1.3
$W^{1p52}S$	−33.8 ± 0.1	3.3 ± 0.3	−48.7 ± 0.7	4.4 ± 0.1	−67.3 ± 1.8*	3.9 ± 0.1
$T^{4p48}A$	−33.7 ± 1.2	3.8 ± 0.5	−51.8 ± 0.5	4.2 ± 0.1	−63.2 ± 1.0*	4.7 ± 0.5
$T^{3i18}A$	−29.6 ± 0.4	4.8 ± 0.2	−53.0 ± 0.3	4.4 ± 0.2	−58.1 ± 1.7	10.9 ± 1.9

SCBI Interaction with Sodium—DCJW, MFZ, and other SCBIs have a conserved fragment N–N–C=O that would chelate a sodium ion to form the energetically preferable 5-membered ring. Such chelating patterns are common. For example, in the gas phase, amino acids form stable 5-membered rings with a sodium ion chelated between the backbone amino and carbonyl groups (33). A sodium ion is readily chelated between the imino nitrogen and ketone oxygen to form a 5-membered ring in picolinic acid (34) and a four-membered ring in cytosine (35).

SCBIs are obviously not strong chelators, and we are not aware of experimental data on association of SCBIs with Na^+, K^+, Ca^{2+}, or other cations in water. However, electroneutral ligands with multiple electronegative atoms should interact with cations within the channel much stronger than in the bulk solvent. Because of specific interactions with the channel proteins, local concentrations of ions and ligands within the channels are much higher than their overall concentrations in the bulk solvent. Therefore, the probability of ligand-metal association within the channel must be much higher than in the bulk

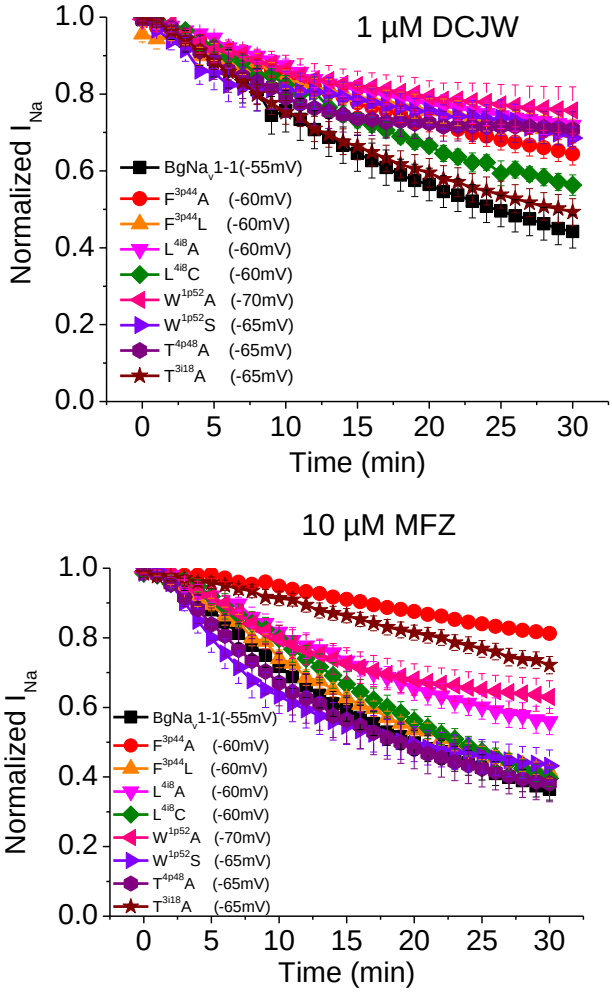

FIGURE 6. **Time course of inhibition of BgNa$_v$1-1a and mutant sodium channels by DCJW (1 μM) and metaflumizone (10 μM).** To measure the inhibition of peak current by SCBIs, test pulses (20 ms) to −10 mV from a depolarizing holding potential (as indicated, *e.g.* −55 mV for BgNa$_v$1-1a) were given once every minute to record the remaining sodium current. The remaining sodium current was then normalized to the current measured prior to application of insecticide. Reduction in *Normalized* I_{Na} reflects the progress of channel inhibition by SCBIs.

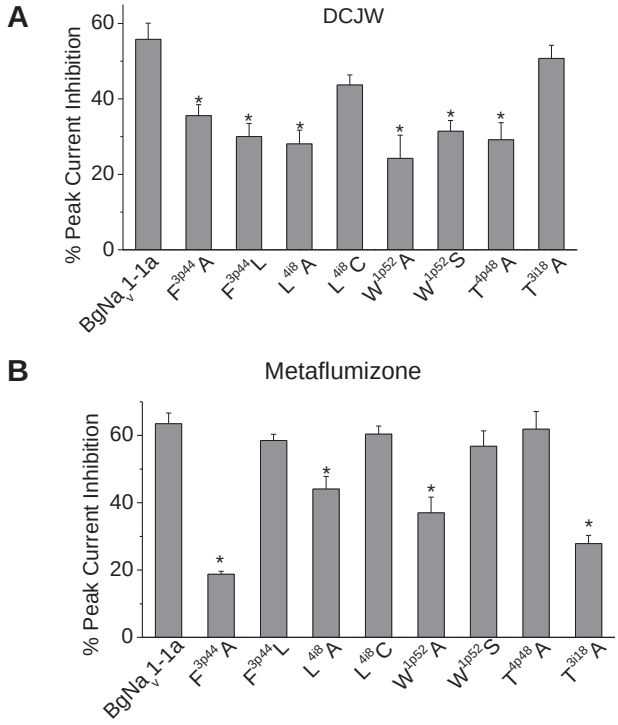

FIGURE 7. **Mutational analysis of SCBI receptors.** Inhibition of peak sodium currents by 1 μM DCJW and (*A*) 10 μM metaflumizone (*B*) at the end of 30 min of incubation, which were calculated from the data in Fig. 6. * means statistically significant.

TABLE 3

Percentage of inhibition of BgNa$_v$1-1a and mutant channels by DCJW (1 μM) and metaflumizone (10 μM) at the end of 30 min of insecticide exposure

The values of percentage of inhibition were determined by values of "normalized I_{Na}" at the end of the 30 min of recording (see Fig. 6). The values represent the mean ± S.E., and the number of oocytes was 6–14. The asterisks indicate significant differences from the BgNa$_v$1-1a channel as determined by one-way ANOVA ($p < 0.05$) with Scheffe's post hoc analysis. Asterisks indicate that the specific residue lines the inner pore and/or specific fenestration.

Na^+ channel	DCJW (1 μM)	Metaflumizone (10 μM)
BgNa$_v$1-1a	55.8 ± 3.8	63.5 ± 2.9
F^{3p44}A	35.6 ± 2.7*	18.7 ± 0.8*
F^{3p44}L	30.0 ± 3.3*	58.5 ± 1.8
L^{4i8}A	28.1 ± 3.5*	44.1 ± 3.7*
L^{4i8}C	43.7 ± 2.3	60.4 ± 2.4
W^{1p52}A	24.2 ± 5.6*	37.0 ± 4.1*
W^{1p52}S	31.4 ± 2.6*	56.8 ± 4.3
T^{4p48}A	29.1 ± 4.1*	61.8 ± 4.8
T^{3i18}A	50.7 ± 3.3	27.8 ± 2.3*

solvent. By the same cause, SCBIs are unlikely to bring a metal ion into the pore from the cytoplasm or extracellular environment, but they would readily associate with a metal ion within the pore.

Structure-Activity Relations of SCBIs—At physiological pH, compound D (Fig. 1) would be protonated. The fact that compound D blocks the sodium channel, although with a weaker potency than classical SCBIs (2), supports the concept that electroneutral SCBIs chelate a sodium ion to form cationic blocking particles. The relatively low potency of compound D is understandable: the ionized ammonium group would reach the imine nitrogen, but not the ketone oxygen so that position of the positive charge would differ from that in DCJW and MFZ. In the series of six RH dihydropyrazoles (Fig. 1), four compounds readily inhibited sodium uptake into mouse brain vesicles, whereas compounds RH5654 and RH2643 were inactive (36). A possible cause is that the hydrophobic butyl group in RH5654 or a partial positive charge in the hydroxy proton of RH2643, which is oriented toward the imino nitrogen, repels a sodium ion from the ligand.

Possible Mechanism of State-dependent Channel Block by LAs and SCBIs—Mutational studies suggest that LAs bind preferably to the fast-inactivation channels (37, 38), but the slow-inactivation states are also considered as targets for the action of LAs (10, 39) and SCBIs (1). A possible cause of this state dependence is that in the inactivated channels the permeant ions would not compete with the pore-bound cationic blockers (13). To some extent, the proposed DCJW binding mode is reminiscent to that of tetracaine, which is predicted to approach the outer pore by the cationic group and extend the other end in the III/IV fenestration (21). The above predictions are consistent with the x-ray structure of the LA-bound Na$_v$Ms

TABLE 4

Organism-specific sodium channel residues, which line the inner pore and fenestrations around repeat IV

Asterisks indicate that the specific residue lines the inner pore and/or specific fenestration.

	Channel		Region		
Position	$Na_v1.4$	$BgNa_v1$-1a	Inner Pore	III/IV fenestration	IV/I fenestration
3p44	Leu	**Phe**		*	
4p47	**Thr**	Ser			*
4i8	**Cys**	Leu	*		
4i11	**Ile**	Leu	*	*	
4i12	**Ile**	Val		*	
3i18	**Val**	Thr		*	
1i19	**Ile**	Val	*		
4i19	Val	**Ile**	*		

channel in which the outer pore is sodium-deficient, and a heavy bromine atom of the ligand is seen in a fenestration (40). Our study proposes common features of the binding modes for cationic LAs and sodium-bound SCBIs in the channel as follows: a positive charge at the focus of P1-helices and a hydrophobic moiety protruding into the III/IV interface.

Another possible explanation for the preferable binding of LAs and SCBIs to the inactivated channels would be a state-dependent three-dimensional complementarity between the ligands and the channel. The pore geometry in the inactivated sodium channels is unknown, and our open-state model is just an approximation to the inactivated state structures. However, the hypothesis on the state-dependent three-dimensional complementarity would not explain why many structurally different ligands of different channels bind preferably to inactivated states. The electrostatic mechanism of the channel block, which assumes competition between ligands and the permeant ions, seems universal to both cationic ligands and metal-bound electroneutral ligands.

Conclusions—In this study we docked DCJW and MFZ in the open-state model of an insect sodium channel. The models predict that the central heterocyclic moiety of SCBIs interacts with a sodium ion in the central cavity, a halogen-substituted aromatic ring extends into the fenestration lined by helices IIIP1, IIS6 and IVS6, and another end of the ligand interacts with the pore helix IP1. Model-driven mutagenesis allowed us to discover five new SCBI-sensing residues, four of which directly interact with the ligands. These include residues in IIIP1 and IVS6, which are specific for insect sodium channels and thus may explain the selective toxicity of MFZ, as well as residues in IVP1 and IIIS6, which interact, respectively, only with DCJW and MFZ. The models imply the channel-blocking mechanism, which is consistent with the hypothesis on direct interactions of electroneutral ligands with permeant ions in the pore of inactivated channels. Because many electroneutral ligands have binding sites that overlap with cationic ligands, the latter conclusion may be of general importance for the pharmacology of ion channels and for developing new selective ligands.

Materials and Methods

Site-directed mutagenesis was performed by PCR using mutant primers and *Pfu* Turbo DNA polymerase (Stratagene, La Jolla, CA). All mutants were verified by DNA sequencing.

Expression of $BgNa_v1$-1a channels in Xenopus laevis Oocytes—The procedures for oocyte preparation and cRNA injection are identical to those described previously (41). For robust expression of the $BgNa_v1$-1a sodium channel, cRNA was co-injected into oocytes with *Drosophila melanogaster* tipE cRNA (1:1 ratio), which enhances the expression of insect sodium channels in oocytes (42, 43).

Electrophysiological Recording and Analysis—Sodium currents were recorded using the two-electrode voltage clamp technique. Electrodes were pulled from borosilicate glass and filled with 3 M KCl and 0.5% agarose. Resistances ranged between 0.5 and 1.5megohms. Currents were measured with an oocyte clamp amplifier OC725C (Warner Instrument Corp., Hamden, CT), Digidata 1440A (Axon Instruments, Foster City, CA), and pClamp 10.2 software (Axon Instruments). Capacitive transient leak currents were subtracted using the P/N ($n = 4$) subtraction method.

Examination of $BgNa_v1$-1a Channel Sensitivity to SCBIs—The methods for measuring the effects of SCBIs on $BgNa_v1$-1a channels are similar to those described previously (17). Briefly, we measured the onset of block by SCBIs at or near the potential of 50% steady-state inactivation. After establishing a stable voltage clamp near the half-inactivation potential specific to a channel variant, insecticide-containing solution was perfused into the bath at a rate of 3 ml/min over the first 7–8 min, and the time course of onset of block was recorded for 30 min. All experiments were performed at room temperature.

Indoxacarb and DCJW were provided by K. D. Wing and D. Cordova (DuPont Agrochemicals), and metaflumizone was provided by Vince Salgado (BASF Agricultural Products). Insecticides were perfused onto oocytes in a manner similar to that previously described (44).

Data are presented as mean ± S.E. Statistical analysis was determined using a one-way analysis of variance test and Scheffe's post hoc analysis. Significance values were set at $p < 0.05$ or as indicated in the table and figure legends.

Molecular Modeling—Sequence alignment of $K_v1.2$ and $BgNa_v1$-1a channels is shown in Fig. 2. Homology modeling and ligand docking were performed using the ZMM program (45) and Monte Carlo-minimization protocol (46) as described elsewhere (6). Molecular images were created using the PyMOL Molecular Graphics System, Version 0.99rc6 (Schrödinger, LLC, New York, NY). We docked S-DCJW because the *R* isomer of indoxacarb is completely inactive (47).

In Silico Opening of the Closed BgNav1-1a Model—We superimposed the closed $BgNa_v1.1$ model with the $K_v1.2$ x-ray structure by minimizing root mean square deviation between the C^α atoms in positions o21, which usually contain small residues Ser, Gly, or Ala (Fig. 2). In both $K_v1.2$ and $BgNa_v1$-1a, o21 residues make close contacts with the H^α backbone atoms in the p40 positions that contain big residues (Phe, Leu, Tyr, or Met). In the superimposed structures (supplemental Fig. S1), the extracellular halves of the P1, S5, and S6 helices overlap rather well. As expected, the cytoplasmic parts did not overlap; the C^α_i30 atoms of the model deviated from the cognate atoms of $K_v1.2$ by 7.6–8.7 Å (supplemental Fig. S1*C*). To open the closed $BgNa_v1$-1a model, we applied centrifugal forces to the C^α_i30 atoms, allowing these atoms (along with the cytoplas-

mic halves of the S6 helices) to move with the step of 0.5 Å and MC-minimized energy at each step as described previously (48). To preserve general folding of the model, we constrained the α-helical H-bonds in helices L45 and the inter-repeat H-bonds between side chains of residues W^{P52} and T/C^{P48} (19).

Unbiased Docking DCJW into the Open $BgNa_v1$-1a Channel—We generated a library of 36 DCJW conformers (supplemental Fig. S4, *A* and *B*) using a force field that disregards the intramolecular van der Waals attractions, thus favoring extended conformations that would interact stronger with the protein (45). Each conformer was docked from 1280 random starting positions/orientations. A total of 36 × 1280 MCM trajectories, each including 10 energy minimizations, were calculated with rigid backbones without imposing any ligand-channel distance constraints.

Biased Docking of Ligands to Experimentally Known Ligand-sensing Residues—This was performed using ligand-side chain distance constraints (49). To preserve the channel folding during docking of flexible ligands to the flexible protein, pin constraints were imposed between matching α-carbons in the template and the model. A pin constraint is a flat-bottom parabolic energy function that allows a C^{α} atom to deviate, penalty-free, up to 1 Å from the template and imposes a penalty of 10 kcal/mol/Å for larger deviations. The pin constraints are necessary because the initial relaxation of the channel model with a bulky ligand would cause large deviations of the protein backbones from the template due to sterical ligand-protein clashes.

Author Contributions—B. S. Z. and K. D. participated in research design. Y. Z., Y. D., Y. N., D. J., C. B., and B. S. Z. conducted experiments and performed data analysis. Y. Z., Y. D., B. S. Z., and K. D. wrote or contributed to the writing of the manuscript.

Acknowledgments—We thank Dr. Kris Silver for critical review of this manuscript and Dr. Denis Tikhonov for helpful discussions. We thank Drs. Keith D. Wing and Daniel Cordova (DuPont Agrochemicals) and Vincent Salgado (BASF Agricultural Products) for providing DCJW and metaflumizone for this study. Computations were performed using the facilities of the Shared Hierarchical Academic Research Computing Network.

References

1. Silver, K. S., Du, Y., Nomura, Y., Oliveira, E. E., Salgado, V. L., Zhorov, B. S., and Dong, K. (2014) in *Advances in Insect Physiology* (Cohen, E., ed) pp. 389–433, Academic Press, Oxford
2. von Stein, R. T., Silver, K. S., and Soderlund, D. M. (2013) Indoxacarb, metaflumizone, and other sodium channel inhibitor insecticides: mechanism and site of action on mammalian voltage-gated sodium channels. *Pestic. Biochem. Physiol.* **106,** 101–112
3. Wing, K. D., Andaloro, J. T., McCann, S. F., and Salgado, V. L. (2005) in *Comprehensive Molecular Insect Science* (L.I., G., Iatrou, K., and Gill, S. S., eds) pp. 31–53, Elsevier, New York
4. Dong, K., Du, Y., Rinkevich, F., Nomura, Y., Xu, P., Wang, L., Silver, K., and Zhorov, B. S. (2014) Molecular biology of insect sodium channels and pyrethroid resistance. *Insect Biochem. Mol. Biol.* **50,** 1–17
5. Rinkevich, F. D., Du, Y., and Dong, K. (2013) Diversity and convergence of sodium channel mutations involved in resistance to pyrethroids. *Pestic. Biochem. Physiol.* **106,** 93–100
6. Du, Y., Nomura, Y., Satar, G., Hu, Z., Nauen, R., He, S. Y., Zhorov, B. S., and Dong, K. (2013) Molecular evidence for dual pyrethroid-receptor sites on a mosquito sodium channel. *Proc. Natl. Acad. Sci. U.S.A.* **110,** 11785–11790
7. Wang, X. L., Su, W., Zhang, J. H., Yang, Y. H., Dong, K., and Wu, Y. D. (2016) Two novel sodium channel mutations associated with resistance to indoxacarb and metaflumizone in the diamondback moth, *Plutella xylostella*. *Insect Sci.* **23,** 50–58
8. Jiang, D., Du, Y., Nomura, Y., Wang, X., Wu, Y., Zhorov, B. S., and Dong, K. (2015) Mutations in the transmembrane helix S6 of domain IV confer cockroach sodium channel resistance to sodium channel blocker insecticides and local anesthetics. *Insect Biochem. Mol. Biol.* **66,** 88–95
9. Silver, K., and Soderlund, D. M. (2005) State-dependent block of rat Nav1.4 sodium channels expressed in *Xenopus* oocytes by pyrazoline-type insecticides. *Neurotoxicology* **26,** 397–406
10. Fozzard, H. A., Lee, P. J., and Lipkind, G. M. (2005) Mechanism of local anesthetic drug action on voltage-gated sodium channels. *Curr. Pharm. Des.* **11,** 2671–2686
11. Mike, A., and Lukacs, P. (2010) The enigmatic drug binding site for sodium channel inhibitors. *Curr. Mol. Pharmacol.* **3,** 129–144
12. Catterall, W. A. (2012) Voltage-gated sodium channels at 60: structure, function and pathophysiology. *J. Physiol.* **590,** 2577–2589
13. Tikhonov, D. B., and Zhorov, B. S. (2007) Sodium channels: ionic model of slow inactivation and state-dependent drug binding. *Biophys. J.* **93,** 1557–1570
14. Lipkind, G. M., and Fozzard, H. A. (2005) Molecular modeling of local anesthetic drug binding by voltage-gated sodium channels. *Mol. Pharmacol.* **68,** 1611–1622
15. Zhorov, B. S., and Tikhonov, D. B. (2004) Potassium, sodium, calcium and glutamate-gated channels: pore architecture and ligand action. *J. Neurochem.* **88,** 782–799
16. Silver, K. S., and Soderlund, D. M. (2007) Point mutations at the local anesthetic receptor site modulate the state-dependent block of rat Na v1.4 sodium channels by pyrazoline-type insecticides. *Neurotoxicology* **28,** 655–663
17. Silver, K. S., Nomura, Y., Salgado, V. L., and Dong, K. (2009) Role of the sixth transmembrane segment of domain IV of the cockroach sodium channel in the action of sodium channel blocker insecticides. *Neurotoxicology* **30,** 613–621
18. Long, S. B., Campbell, E. B., and Mackinnon, R. (2005) Crystal structure of a mammalian voltage-dependent Shaker family K^+ channel. *Science* **309,** 897–903
19. Payandeh, J., Scheuer, T., Zheng, N., and Catterall, W. A. (2011) The crystal structure of a voltage-gated sodium channel. *Nature* **475,** 353–358
20. Zhorov, B. S., and Tikhonov, D. B. (2013) Ligand action on sodium, potassium, and calcium channels: role of permeant ions. *Trends Pharmacol. Sci.* **34,** 154–161
21. Bruhova, I., Tikhonov, D. B., and Zhorov, B. S. (2008) Access and binding of local anesthetics in the closed sodium channel. *Mol. Pharmacol.* **74,** 1033–1045
22. Zhang, X., Ren, W., DeCaen, P., Yan, C., Tao, X., Tang, L., Wang, J., Hasegawa, K., Kumasaka, T., He, J., Wang, J., Clapham, D. E., and Yan, N. (2012) Crystal structure of an orthologue of the NaChBac voltage-gated sodium channel. *Nature* **486,** 130–134
23. McCusker, E. C., Bagnéris, C., Naylor, C. E., Cole, A. R., D'Avanzo, N., Nichols, C. G., and Wallace, B. A. (2012) Structure of a bacterial voltage-gated sodium channel pore reveals mechanisms of opening and closing. *Nat. Commun.* **3,** 1102
24. Naylor, C. E., Bagnéris, C., DeCaen, P. G., Sula, A., Scaglione, A., Clapham, D. E., and Wallace, B. A. (2016) Molecular basis of ion permeability in a voltage-gated sodium channel. *EMBO J.* **35,** 820–830
25. Hille, B. (1977) Local anesthetics: hydrophilic and hydrophobic pathways for the drug-receptor reaction. *J. Gen. Physiol.* **69,** 497–515
26. Du, Y., Garden, D. P., Wang, L., Zhorov, B. S., and Dong, K. (2011) Identification of new batrachotoxin-sensing residues in segment IIIS6 of the sodium channel. *J. Biol. Chem.* **286,** 13151–13160
27. Tikhonov, D. B., and Zhorov, B. S. (2005) Sodium channel activators: model of binding inside the pore and a possible mechanism of action. *FEBS Lett.* **579,** 4207–4212

28. Zhou, Y., Morais-Cabral, J. H., Kaufman, A., and MacKinnon, R. (2001) Chemistry of ion coordination and hydration revealed by a K^+ channel-Fab complex at 2.0 A resolution. *Nature* **414,** 43–48
29. Omae, I. (2004) Intramolecular five-membered ring compounds and their applications. *Coordination Chemistry Reviews* **248,** 995–1023
30. Bruhova, I., and Zhorov, B. S. (2005) KvAP-based model of the pore region of shaker potassium channel is consistent with cadmium- and ligand-binding experiments. *Biophys. J.* **89,** 1020–1029
31. Korkosh, V. S., Zhorov, B. S., and Tikhonov, D. B. (2016) Analysis of inter-residue contacts reveals folding stabilizers in P-loops of potassium, sodium, and TRPV channels. *Eur. Biophys. J.* **45,** 321–329
32. Tikhonov, D. B., Bruhova, I., and Zhorov, B. S. (2006) Atomic determinants of state-dependent block of sodium channels by charged local anesthetics and benzocaine. *FEBS Lett.* **580,** 6027–6032
33. Talley, J. M., Cerda, B. A., Ohanessian, G., and Wesdemiotis, C. (2002) Alkali metal ion binding to amino acids *versus* their methyl esters: affinity trends and structural changes in the gas phase. *Chemistry* **8,** 1377–1388
34. Ohanessian, G. (2002) Interaction of MALDI matrix molecules with Na^+ in the gas phase. *Int. J. Mass Spectrom.* **219,** 577–592
35. Wang, P., Polce, M. J., Ohanessian, G., and Wesdemiotis, C. (2008) The sodium ion affinities of cytosine and its methylated derivatives. *J. Mass Spectrom.* **43,** 485–494
36. Payne, G. T., Deecher, D. C., and Soderlund, D. M. (1998) Structure-activity relationships for the action of dihydropyrazole insecticides on mouse brain sodium channels. *Pestic. Biochem. Physiol.* **60,** 177–185
37. Bennett, P. B., Valenzuela, C., Chen, L. Q., and Kallen, R. G. (1995) On the molecular nature of the lidocaine receptor of cardiac Na^+ channels. Modification of block by alterations in the α-subunit III-IV interdomain. *Circ. Res.* **77,** 584–592
38. Balser, J. R., Nuss, H. B., Orias, D. W., Johns, D. C., Marban, E., Tomaselli, G. F., and Lawrence, J. H. (1996) Local anesthetics as effectors of allosteric gating. Lidocaine effects on inactivation-deficient rat skeletal muscle Na channels. *J. Clin. Invest.* **98,** 2874–2886
39. Balser, J. R., Nuss, H. B., Romashko, D. N., Marban, E., and Tomaselli, G. F. (1996) Functional consequences of lidocaine binding to slow-inactivated sodium channels. *J. Gen. Physiol.* **107,** 643–658
40. Bagnéris, C., DeCaen, P. G., Naylor, C. E., Pryde, D. C., Nobeli, I., Clapham, D. E., and Wallace, B. A. (2014) Prokaryotic NavMs channel as a structural and functional model for eukaryotic sodium channel antagonism. *Proc. Natl. Acad. Sci. U.S.A.* **111,** 8428–8433
41. Tan, J., Liu, Z., Tsai, T. D., Valles, S. M., Goldin, A. L., and Dong, K. (2002) Novel sodium channel gene mutations in *Blattella germanica* reduce the sensitivity of expressed channels to deltamethrin. *Insect. Biochem. Mol. Biol.* **32,** 445–454
42. Feng, G., Deák, P., Chopra, M., and Hall, L. M. (1995) Cloning and functional analysis of tipE, a novel membrane protein that enhances drosophila *para* sodium channel function. *Cell* **82,** 1001–1011
43. Warmke, J. W., Reenan, R. A., Wang, P., Qian, S., Arena, J. P., Wang, J., Wunderler, D., Liu, K., Kaczorowski, G. J., Van der Ploeg, L. H., Ganetzky, B., and Cohen, C. J. (1997) Functional expression of *Drosophila para* sodium channels–Modulation by the membrane protein TipE and toxin pharmacology. *J. Gen. Physiol.* **110,** 119–133
44. Tatebayashi, H., and Narahashi, T. (1994) Differential mechanism of action of the pyrethroid tetramethrin on tetrodotoxin-sensitive and tetrodotoxin-resistant sodium channels. *J. Pharmacol. Exp. Ther.* **270,** 595–603
45. Garden, D. P., and Zhorov, B. S. (2010) Docking flexible ligands in proteins with a solvent exposure- and distance-dependent dielectric function. *J. Comput. Aided Mol. Des.* **24,** 91–105
46. Li, Z., and Scheraga, H. A. (1987) Monte Carlo-minimization approach to the multiple-minima problem in protein folding. *Proc. Natl. Acad. Sci. U.S.A.* **84,** 6611–6615
47. McCann, S. F., Annis, G. D., Shapiro, R., Piotrowski, D. W., Lahm, G. P., Long, J. K., Lee, K. C., Hughes, M. M., Myers, B. J., Griswold, S. M., Reeves, B. M., March, R. W., Sharpe, P. L., Lowder, P., Barnette, W. E., and Wing, K. D. (2001) The discovery of indoxacarb: oxadiazines as a new class of pyrazoline-type insecticides. *Pest Manag. Sci.* **57,** 153–164
48. Tikhonov, D. B., and Zhorov, B. S. (2004) *In silico* activation of KcsA K^+ channel by lateral forces applied to the C termini of inner helices. *Biophys. J.* **87,** 1526–1536
49. Du, Y., Nomura, Y., Zhorov, B. S., and Dong, K. (2016) Evidence for dual binding sites for DDT in insect sodium channels. *J. Biol. Chem.* **291,** 4638–4648
50. Tikhonov, D. B., and Zhorov, B. S. (2012) Architecture and pore block of eukaryotic voltage-gated sodium channels in view of NavAb bacterial sodium channel structure. *Mol. Pharmacol.* **82,** 97–104
51. von Stein, R. T., and Soderlund, D. M. (2012) Compound-specific effects of mutations at Val787 in DII-S6 of Nav 1.4 sodium channels on the action of sodium channel inhibitor insecticides. *Neurotoxicology* **33,** 1381–1389
52. von Stein, R. T., and Soderlund, D. M. (2012) Role of the local anesthetic receptor in the state-dependent inhibition of voltage-gated sodium channels by the insecticide metaflumizone. *Mol. Pharmacol.* **81,** 366–374
53. Ragsdale, D. S., McPhee, J. C., Scheuer, T., and Catterall, W. A. (1994) Molecular determinants of state-dependent block of Na+ channels by local anesthetics. *Science* **265,** 1724–1728